Dimethyl sulfide (DMS) climatologies, fluxes, and trends - Part B: Sea-air fluxes

Sankirna D. Joge[1,2], Anoop S. Mahajan[1, *], Shrivardhan Hulswar[1], Christa A. Marandino[3], Martí Galí[4,5], Thomas G. Bell[6], Mingxi Yang[6] and Rafel Simo[4]

[1]Indian Institute of Tropical Meteorology, Pune, India

[2]Savitribai Phule Pune University, Pune, India

[3]Research Division 2-Biogeochemistry, GEOMAR Helmholtz Centre for Ocean Research Kiel, Kiel, Germany

[4]Institut de Ciències del Mar (CSIC), Barcelona, Catalonia, Spain

[5] Barcelona Supercomputing Center (BSC), Barcelona, Spain

[6]Plymouth Marine Laboratory (PML), Plymouth, UK

*Correspondence to: Anoop S. Mahajan (anoop@tropmet.res.in)

Abstract. Dimethyl sulfide (DMS) contributes to cloud condensation nuclei (CCN) formation in the marine environment. DMS is ventilated from the ocean to the atmosphere, and in most models, this flux is calculated using seawater DMS concentrations and a sea-air flux parameterization. Here, climatological seawater DMS concentrations from interpolation and parameterization techniques are passed through seven flux parametrizations to estimate the DMS flux. The seasonal means of calculated fluxes are compared to identify differences in absolute values and spatial distribution, which show large differences depending on the flux parameterization used. In situ flux observations were used to validate the estimated fluxes from all seven parameterizations. Even though we see a correlation between the estimated and observation values, all methods underestimate the fluxes in the higher range (>20 µmol m^{-2} d^{-1}) and overestimate the fluxes in the lower range (< 20 µmol m^{-2} d^{-1}). The estimated uncertainty in DMS fluxes is driven by the uncertainty in seawater DMS concentrations in some regions but by the choice of flux parameterization in others. We show that the resultant flux is hence highly sensitive to both and suggest that there needs to be an improvement in the estimation methods of global seawater DMS concentration and sea-air fluxes for accurately modeling the effect of DMS on the atmosphere.

1 Introduction

Dimethyl Sulfide (DMS) is a volatile organic compound obtained from its precursor dimethylsulfoniopropionate (DMSP) through enzymatic cleavage (Andreae and Crutzen, 1997; Charlson et al., 1987; Simó, 2001; Yang et al., 2014; Abbatt et al., 2019; Galí and Simó, 2015). In seawater, DMS further undergoes biotic and abiotic processes. It is consumed by three major processes: (1) bacterial decomposition, (2) photolysis and, (3) ventilation to the atmosphere (Del Valle et al., 2009; Xu et al., 2019; Zhai et al., 2020). The last process is important as DMS in the atmosphere contributes to the formation of cloud

condensation nuclei (CCN). Once DMS is released into the atmosphere from the sea surface, it is oxidized by hydroxyl radicals (OH), nitrate radical (NO_3) and halogen radicals (Br and Cl) to form sulfur dioxide (SO_2), methane sulfonic acid, and gas-phase sulphuric acid, which contribute to the formation of CCN (Andreae and Barnard, 1984; Woodhouse et al., 2010; Pazmiño et al., 2005). Hence, DMS has importance in cloud formation, and affects the climate due to its direct and indirect effect on radiative forcing (Yoch, 2002), although some uncertainties remain about its overall impacts and climate feedback (Quinn and Bates, 2011; Quinn et al., 2017).

Although the oceans are the major source of global DMS emissions, minor amounts of DMS has also been found to be emitted from vegetation on land (Vettikkat et al., 2020; Jardine et al., 2015; Yi et al., 2008). However, DMS emitted from the surface ocean is responsible for up to 70 % of the natural sulfur emissions into the global atmosphere (Andreae and Raemdonck, 1983; Carpenter et al., 2012; Hulswar et al., 2022). Considering this, it is important to develop a precise emission inventory for the assessment of climate impacts due to DMS emissions (Mahajan et al., 2015; Yang et al., 2015, 2017; Jin et al., 2018).

The emission of DMS occurs due to differences in concentrations of DMS in the seawater and the atmosphere. The sea-air gas transfer is a complex process, with the wind proven to be one of the most influencing factors (Jahne et al., 1979; Frew et al., 2004; D'Asaro and McNeil, 2008; Blomquist et al., 2017). For example, DMS flux measurements have revealed a decrease in gas transfer at medium to high wind speeds (> 10 m s^{-1}), attributed to wave-wind interactions and surfactant effects (Zavarsky et al., 2018), factors typically overlooked in traditional approaches (Bell et al., 2017).Hence, the sea-air gas transfer is parameterized as a function of wind speed. In an earlier comparison, Kettle and Andreae (Kettle and Andreae, 2000) compared three parametrizations viz., Liss & Merlivat (1986), Wanninkhof (1992), and Erickson (1993). They concluded that uncertainty in the flux parameterizations leads to uncertainties in estimating the global DMS flux. Furthermore, different datasets for wind speed, sea surface temperature (SST), and sea surface DMS concentration resulted in relatively small variations in these calculated fluxes (≤ 25 %) (Kettle and Andreae, 2000).

Here, we compare global sea-air DMS fluxes derived using seven different gas transfer velocity parameterizations using wind speed and SST. The comparison is conducted using different seawater DMS estimations to identify whether the uncertainty in the emissions is larger because of the uncertainty in seawater DMS concentrations or the flux parameterization. We use one interpolation-based seawater DMS concentration climatology ((Hulswar et al., 2022), hereafter referred to as H22) and two parameterization-based seawater DMS climatologies (Galí et al. (2018), hereafter referred to as G18 and Wang et al. (2020), hereafter referred to as W20). A comparison between the three seawater DMS climatologies is presented in the sister paper (Joge et al., referred to as Joge: Part A). The comparison shows that there is a large difference between the interpolation and proxy-based parameterization methods of estimating seawater DMS concentrations, with the interpolation-based method predicting higher values. Interestingly, both methods show an increase in DMS emissions over the last two decades. Here, we inter-compared the DMS fluxes estimated using seven sea-air flux parameterizations and in situ DMS fluxes and identified the drivers of their uncertainties.

2 Data and methodology

For DMS flux calculation, seven parametrization schemes (LM86 (Liss and Merlivat, 1986), E93 (Erickson, 1993), N00a, N00b (Nightingale et al., 2000), Ho06 (Ho et al., 2006), GM12 (Goddijn-Murphy et al., 2012), W14 (Wanninkhof, 2014)) are
65   used with the seawater DMS climatological data of H22, G18, and W20 (please check Joge: Part A for a comparison between the seawater DMS estimations). Each flux parametrization scheme uses wind speed, and some also use SST to estimate the DMS sea-air flux. Wind speed and SST were obtained from the National Centers for Environmental Prediction (NCEP; https://psl.noaa.gov/data/gridded/index.html) (Kalnay et al., 1996) and Centennial in situ Observation-Based Estimates (COBE; https://psl.noaa.gov/data/gridded/data.cobe.html) (Ishii et al., 2005), respectively, for the years from 1948 to 2022,
70   and then monthly averaged to calculate the fluxes. The in situ DMS flux observations measured by eddy covariance or gradient flux techniques were obtained from various studies carried out over the global oceans (Table S1). The corresponding locations of flux observation data are shown in Fig. S12.

In general, all the parameterizations we compare in this study depend on wind speed (u) and the Schmidt number (Sc), which depends on temperature (T). The Schmidt number (Sc) is a dimensionless number defined as the ratio of momentum diffusivity
75   (v) and mass diffusivity (D), i.e., $Sc = v/D$ (Liss and Merlivat, 1986). The DMS sea-air flux is determined by using a bulk flux equation $F = k(C_w - C_a/H)$ where F is the calculated DMS flux, k is the gas transfer velocity, and C_w and C_a are the concentrations of the DMS in the seawater and the atmosphere adjacent to the seawater respectively (Wanninkhof, 2014). H is Henry's law solubility for DMS in seawater, which varies with temperature, which is given as $ln\ H = -3547/T +12.64$ (Dacey and Wakeham, 1984). Here, C_a and C_w are measured in situ, while k depends on wind speed. C_w is several orders of magnitude
80   higher than C_a; hence C_a/H is often ignored (Yan et al., 2023). It should be noted that previous studies have shown that C_a becomes important when the atmospheric boundary layer is shallow and surface concentration is high (Steiner et al., 2006; Steiner and Denman, 2008). The flux parameterization methods give estimates of the k and Sc values, and we follow $F = kC_w$ for DMS flux estimation with all seven flux parametrizations.

As wind is one of the most influential factors affecting gas transfer, most parameterizations have established different wind
85   speed regimes for which different equations estimate the k values (Liss and Merlivat, 1983; Erickson, 1993). The gas transfer velocity k results from the waterside transfer velocity (k_w) and airside transfer velocity (k_a). For the rarely soluble gas, airside resistance is usually small and neglected, but DMS solubility increases with a decrease in temperature, and hence, air resistance becomes important (Lana et al., 2011; Marandino et al., 2009; Omori et al., 2017). Most parameterizations agree that at wind speeds less than 3.6 m s^{-1}, the surface is generally smooth with few waves, known as the 'smooth surface regime.' When the
90   wind speed is above 3.6 m s^{-1} but less than 13 m s$^{-1,}$ it is 'rough surface regime,' and more waves can be seen, enhancing the gas transfer. Above 13 m s^{-1} is known as the 'breaking wave regime,' where bubbles are formed along with the waves, dominant increasing the flux as evident from the Heidelberg circular wind tunnel experiments (Jähne et al., 1984; Jahne et al., 1979; Liss and Merlivat, 1986). The different flux parameterizations estimate the k value in those different wind regimes ($u \leq 3.6$: smooth

surface regime, $3.6 < u \leq 13$: rough surface regime, $u > 13$: breaking wave regime), and these wind regimes are also dependent on the Schmidt number (Sc) for each parametrization, where Schmidt number depends on temperature (T).

2.1 Flux parameterization methods

2.1.1 LM86 Flux Parametrization

LM86 formulated the following equations for the three wind regimes, which are defined below following the results of the Heidelberg experiments (Jahne et al., 1979; Jähne et al., 1984) :

$$k_{lm86} = 0.17 \times \left(600/Sc\right)^{2/3} \times u \qquad\qquad (u \leq 3.6) \qquad\qquad (1)$$

$$k_{lm86} = \left(600/Sc\right)^{1/3} \times (2.85 \times u - 10.26) + 0.61 \times \left(600/Sc\right)^{2/3} \qquad (3.6 < u \leq 13) \qquad (2)$$

$$k_{lm86} = \left(600/Sc\right)^{1/3} \times (5.9 \times u - 49.91) + 0.61 \times \left(600/Sc\right)^{2/3} \qquad (u > 13) \qquad (3)$$

Here, u is the wind speed in m s^{-1} at 10 m above the sea surface. The Sc is based on the work carried out by Saltzman *et al.* (1993) and the references therein for the temperature range from 5° C to 30° C using:

$$Sc = 2674 - (147.12 \times SST) + (3.726 \times SST^2) - (0.038 \times SST^3) \qquad\qquad (4)$$

The k_{lm86} vs u plot for all the months is shown in Fig.S1. From the figure it can be seen that gas transfer coefficient varies as a linear function of u. The three wind regimes defined by Eq. 1-3 can be seen in June, July and August months and the spread of k_{lm86} is due to the dependence of Schmidt number (Sc) on SST.

2.1.2 E93 Flux Parameterization

Erickson (1993) assumed that the sea surface is a mixture of a low-turbulence area (non-whitecap) and a high-turbulence area (whitecap). The gas transfer velocities are obtained from the radon outgassing data obtained during the expedition of Transient Tracers in the Ocean (TTO) and Geochemical Ocean Sections Study (GEOSECS) (Monahan and Spillane, 1984; Kettle and Andreae, 2000). The gas transfer velocities for other species are calculated using the following conversion formula based on wind speed ranges:

$$k_{e93} = k_{Rn} \times \left(Sc/Sc_{Rn}\right)^{-2/3} \qquad\qquad (u < 3.6) \qquad\qquad (5)$$

$$k_{e93} = k_{Rn} \times \left(Sc/Sc_{Rn}\right)^{-1/3} \qquad\qquad (u \geq 3.6) \qquad\qquad (6)$$

Here, k_{Rn} (Monahan and Spillane, 1984) and Sc_{Rn} are the gas transfer velocity and Schmidt number for radon, respectively, which are given as follows:

$$k_{Rn} = 2.3 + 1.25 \times 10^{-3} \times u^3 \qquad\qquad (u \text{ in m d}^{-1}) \qquad\qquad (7)$$

120 $$Sc_{R_n} = 3147.3 - 201.9 \times SST + 5.5 \times SST^2 - 0.055 \times SST^3 \tag{8}$$

The k_{e93} vs u plot for all the months is shown in Fig.S2. The gas transfer coefficient varies as a cube of u (Eq.7). The spread of k_{e93} with u is due to the dependence of Schmidt number (Sc) on SST but this spread is not as much as it can be seen in other plots (Figs.S1, S3, S4, S6 and S7).

2.1.3 N00a and N00b Flux Parametrization

125 Dual tracer methods involving the measurements of sulfur hexafluoride SF_6 and 3-Helium (^{3}He) were also used to estimate k (Watson et al., 1991). Nightingale et al. (2000) describe the ideal dual tracer combination as the one with one of the tracers being non-volatile, allowing dilution and dispersion corrections to be applied to the volatile tracer to minimize errors while estimating k. Due to the absence of such an ideal marine tracer, Nightingale et al. (2000) introduced a novel method of adding metabolically inactive bacterial spores of *Bacillus globigii* var. *Niger* as a conservative tracer to study the gas exchange in the

130 North Sea (Watson et al., 1991; Nightingale et al., 2000) along with SF_6 and ^{3}He dual tracer for comparison. Combining data from other studies in George's Bank (Wanninkhof et al., 1993) and the West Florida shelf (Wanninkhof et al., 1997) with the North Sea data, the N00a parameterization coefficient was given as

$$k_{n00a} = (0.222 \times u^2 + 0.333 \times u) \times \left(Sc/600\right)^{-0.5} \tag{9}$$

However, this study exclusively had data from the Northern Atlantic region. Coale et al. (1996) reported k values by using the

135 dual tracer ($SF_6/^3$He) in the equatorial Pacific Ocean, which was then used to upgrade the N00a parameterization to N00b; the upgraded parameterization is given as

$$k_{n00b} = (0.222 \times u^2 \times shape\ parameter + 0.333 \times u) \times \left(Sc/600\right)^{-0.5} \tag{10}$$

Here, the *shape parameter* is used to describe variations in wind speed using Weibull Distribution (Waewsak et al., 2011). Both the parametrizations depend on Schmidt number (Sc) and hence spread in the values are present (Figs. S3 and S4). Also,

140 k_{n00a} and k_{n00b} varies as u and u^2 (Eq. 9 and 10) which can also be seen in both figures.

2.1.4 Ho06 Flux Parameterization

Ho et al. (2006) applied the dual tracer technique to measure the gas transfer velocity with the wind speed ranging from 7–16 m s^{-1}. This was done during the Surface Ocean Lower Atmosphere Study (SOLAS) Air-Sea Gas Exchange (SAGE) campaign. The estimation of Ho06 was derived from the SAGE data, and the gas transfer coefficient is given as,

145 $$k_{ho06} = (0.266 \pm 0.019) \times u^2 \tag{11}$$

The k_{ho06} is not dependent on Schmidt number but depends upon u^2. Hence, the spread is negligible and it is exponentially varying with increase in wind speed (u) (Fig. S5).

2.1.5 GM12 Flux Parametrization

150   Goddijn-Murphy et al. (Goddijn-Murphy et al., 2012) argued that since the wind does not directly affect the gas transfer, it is the turbulence caused due to wind that helps to form bubbles, which increases gas transfer. Hence, the sea-surface roughness is a better parameter to quantify gas transfer. This study used satellite altimetry data to understand the sea surface roughness and measured DMS gas transfer velocity using the eddy covariance flux determination from eight cruises. This resulted in the new GM12 parameterization, which gives gas transfer velocity given as,

155    $k_{gm12} = (2.1 \times u - 2.8) \times \left(Sc/660\right)^{-0.5}$ (12)

From k_{gm12} vs u plot (Fig. S6), it can be seen that k_{gm12} varies linearly with u along with the spread in values as it also varies with Schmidt number (*Sc*) (Eq. 12).

2.1.6 W14 Flux Parametrization

Wanninkhof (1992) used the radiocarbon ^{14}C data from the Red Sea (Cember, 1989) to understand the CO_2 gas exchange rates.

160   Based on this, the parametrization was developed using *Sc* number related to the work carried out by Saltzman *et al.* (1993) with the temperature range between 18º C to 25º C. Further, with the help of better quantification of global wind fields and using data with a broader temperature range (-2º C to 40º C), the parametrization developed in 1992 is being upgraded using revised global ocean ^{14}C inventories and an improved wind speed product (Wanninkhof, 2014). This new parametrization technique is known as W14, which gives a gas transfer velocity equation:

165    $k_{w14} = 0.251 \times u^2 \times \left(Sc_{w14}/660\right)^{-0.5}$ (13)

Here:

$Sc_{w14} = 2855.7 - 177.63 \times SST + 6.0438 \times SST^2 - 0.11645 \times SST^3 + 0.00094743 \times SST^4$ (14)

The k_{w14} vs u plot is shown in Fig. S7 for all the months. The values vary as a function of u^2 along with the spread due to Sc_{w14}.

170   The *k* vs *u* plots of all above mentioned parametrization methods is shown in supplementary text (Figs. S1-S7). Here, we compare the seven flux parametrization methods for piston velocity (k). Further, the *k* values of all seven parametrizations are used to estimate uncertainty in the parameterizations and hence, the resulting flux.

2.2 Estimation of uncertainties

175   The total uncertainty in DMS fluxes (σ_{total}) is calculated using the standard deviations in seawater DMS concentration (σ_{DMS}), coefficient of parameterization (σ_k), and wind speed (σ_{wind}):

$$\sigma_{total} = \sqrt{\sigma_{DMS}^2 + \sigma_k^2 + \sigma_{wind}^2} \qquad\qquad (15)$$

Here, σ_{DMS} is calculated by calculating standard deviation between H22, W20 and G18. This σ_{DMS} is used along with N00a parametrization, windspeed and SST data to estimate the standard deviation in the flux, which is shown in monthly and annual σ_{DMS} plots (Fig. S10). Next, σ_k is calculated by calculating standard deviation between k from all seven flux parametrization equations and this σ_k is further used along with H22 seawater DMS climatology data, windspeed and SST data to get standard deviation in flux which is shown in the monthly and annual σ_k plot (Fig. S11). Similarly, σ_{wind} is calculated by calculating standard deviation between monthly global wind data from the different sources (NCEP Reanalysis 1, NCEP/DOE Reanalysis 2, ECMWF Reanalysis v5 (ERA5)) and it is used along with N00a parametrization, H22 seawater DMS climatology data and SST to calculate standard deviation in flux (plot is not shown however, area weighted global mean is shown in Table 1). In this analysis, N00b is chosen as it has been used for previous DMS studies (Simó and Dachs, 2002; McNabb and Tortell, 2022; Zhang et al., 2021; Zhao et al., 2003, 2024; Lana et al., 2011; Hulswar et al., 2022) for the calculation of fluxes. Finally, σ_{total} is obtained using Eq.(15).

3 Results

3.1 Salient features and seasonal variations

We estimated the seasonal DMS flux using seven different parameterizations and the global seawater DMS data of H22 (Fig.1), G18 (Fig.S8), and W20 (Fig.S9) climatologies to study the geographical and seasonal variations and the differences between the parameterizations.

Overall, the fluxes estimated using all seven parameterizations follow the seawater DMS concentration distribution, with higher values in the southern/northern hemispheres during their respective summers (Fig.1). Elevated levels are also seen in the Indian, Atlantic, and Pacific Oceans in the extra-tropical regions, where elevated wind speed causes higher sea-air fluxes. While the geographical patterns are similar, there is a large difference in the absolute values among the different parameterizations. When using the G18 or W20 seawater DMS concentrations, the emissions show a similar difference among the different parameterizations, although the absolute values are lower (Fig.S8 and S9).

In December-January-February (DJF), E93 shows a maximum DMS flux of 45.82 µmol m^{-2} d^{-1} in the Weddell Sea region, where the maximum DMS concentration of 18.67 nM is also calculated in H22 (Joge: Part A). For E93, the flux is more uniformly distributed across the Southern Ocean as compared to the other parameterizations (Fig. 1). The other parameterizations also show elevated values in the Southern Ocean, although the range depends on the parameterization used. For example, the E93 parameterization results in the highest values, exceeding 20 µmol m^{-2} d^{-1} throughout the Southern Ocean, while the LM86 parameterization results in peak values less than 10 µmol m^{-2} d^{-1}. Further north, in other ocean basins such as the Indian Ocean Ho06, and N00b predict relatively higher fluxes than E93.

During March-April-May (MAM), most parameterizations lead to elevated fluxes in the North Atlantic Ocean, Caribbean Sea, Baltic Sea, and North Sea, with the DMS flux ranging from 8.71 to 18.73 µmol m^{-2} d^{-1} using the H22 seawater DMS concentrations. Higher fluxes are also calculated on the western coast of the American continent and in the coastal regions of Africa. The gyres in the equatorial Pacific and Indian Oceans also show higher fluxes, although the Northern Atlantic Ocean has higher fluxes than the other ocean basins. Although all the parameterizations show higher values in the northern hemisphere, E93 shows the highest fluxes, and the LM86 parameterization shows the lowest fluxes. In a similar manner, N00b shows high flux values (13.8 µmol m^{-2} d^{-1}) compared to N00a (11.33 µmol m^{-2} d^{-1}) in the Caribbean Sea, probably due to the wind correction factor in the N00b parametrization.

The June-July-August (JJA) period shows high values in the upwelling regions off the continental coasts and the equatorial Indian Ocean and Pacific Ocean. During this period, the geographical variation strongly depends on the parameterization chosen. For example, the E93 parameterization mainly shows peaks in the Arctic Ocean and the northern boundaries of the other ocean basins. However, other parameterizations show peaks in the equatorial oceans in addition to the northern latitudes. This difference in variation is driven by the different responses of the parameterizations to winds.

Flux values start increasing in the Southern Ocean during September-October-November (SON). The flux value estimated by Ho06 were the highest during this period (18.40 µmol m^{-2} d^{-1}) in the south Atlantic Ocean along coastal areas of South Africa, although the other parameterizations also show an increase in the Southern Ocean except for LM86. A distinct hotspot is also seen in the Indian Ocean region in all estimations such as Ho06 followed by N00a (13.77 µmol m^{-2} d^{-1}), N00b (16.75 µmol m^{-2} d^{-1}), GM12 (11.97 µmol m^{-2} d^{-1}), and W14 (13.84 µmol m^{-2} d^{-1}), while LM86 estimated the least (10.66 µmol m^{-2} d^{-1}) in the Indian ocean region.

3.2 Differences

We calculated the seasonal differences between all the flux parameterizations with respect to the N00b (Fig.2), however DMS-CO2 flux usually uses W14 flux parametrization but we choose N00b as it is used in the recent DMS climatology papers (Wang et al., 2020; Hulswar et al., 2022; Lana et al., 2011; Zhao et al., 2024). Annually, the largest positive difference is seen in the LM86 parameterization, which consistently displays lower values than the N00b parametrization due to linear dependence of windspeed in LM86 and quadratic in N00b (Eq. 1-3 and Eq.10). The largest negative differences in the polar regions are present in the E93 parameterization, which shows that higher values are calculated at those regions than the N00b parameterization. Although Ho06 also shows large negative differences in the polar regions, large positive differences are present in the mid-latitude and coastal regions. These differences can be as much as 100 % in certain regions, showing that the choice of parameterization plays a crucial role in the DMS flux estimates. The largest positive differences are present in N00b - LM86 in all the seasons, while the largest negative differences can be seen with N00b - E93 (Fig 2). This large negative difference is driven by the differences in the high latitude regions where N00b does not show peaks, for example, in the Southern Ocean (Fig. 1). In the mid-latitude and the equatorial regions, peaks are present in N00b estimations and hence N00b - E93 shows the largest positive differences as listed in Table S2. Although N00b is upgraded from N00a parameterization,

there is no negative difference between the two parametrizations (Fig.2), which indicates that N00b estimates higher flux values than N00a (Fig. 1). The maximum positive differences between the two is listed in Table S2 for all seasons. The differences between N00b and Ho06 are primarily negative (Table S2), but the positive differences are also present in the range from 1.5 to 2.37 μmol m^{-2} d^{-1} but lower than N00b - N00a. The difference between N00b and GM12 is positive. Similarly, in the case of N00b - W14, positive differences are present which can be clearly seen from Fig. 2. The summary of the maximum positive and negative values of differences in different oceanic regions is given in Table S2 of supplementary text.

3.3 Drivers in flux uncertainties

As explained in the methods section, the total uncertainty in DMS fluxes is derived from the uncertainty in the seawater DMS concentrations, parameterization, and wind speed.

Fig.S10 shows the standard deviation in the DMS flux calculated using the standard deviation between climatological seawater DMS concentrations (σ_{DMS}) of G18, W20, and H22. Here, the sea-air parameterization is kept constant to isolate the effect of the change due to seawater DMS concentrations. The monthly climatological wind speed data (NCEP reanalysis 1) is used for the flux estimation. From Table S3 the maximum σ_{DMS} can be seen in December, January and February in South Atlantic Ocean compared to June, July and August months in North Atlantic Ocean and Arabian Sea. Overall, the largest standard deviation in σ_{DMS} can be seen in the Southern Ocean (Fig. S10), where the DMS concentrations are the largest. Fig.S11 shows the standard deviation in the DMS flux due to the standard deviation among seven gas transfer velocity coefficients (σ_k). Here, we keep the seawater DMS concentrations constant (H22), and monthly climatological wind speed data of NCEP reanalysis 1 is used. The maximum σ_k can be seen in December, January and February in Weddell Sea region compared to June, July and August months in Indian Ocean region (Table S3 in supplementary text). From Fig.S10 and Fig.S11, it can be compared that σ_k is dominant over σ_{DMS} in Weddell Sea region as well as across the coast of Antarctic region. Apart from this coastal region in Antarctica, other coastal regions are dominated by σ_{DMS}.

Further, the standard deviation in the DMS flux is estimated by calculating standard deviation in wind speed (σ_{wind}) obtained from different sources. The area weighted global mean flux standard deviation due to σ_{wind} is much lower than the area weighted global mean flux standard deviation due to σ_{DMS} and σ_k on monthly and annual scales (Table 1). Also, from Table S3, it can be seen that maximum σ_{wind} is less in all the months and on the annual scale compared to σ_{DMS} and σ_k; even though these values are from different oceanic regions. This shows that the total standard deviation of the sea-air DMS flux (σ_{total}) is dominated by σ_{DMS} and σ_k, with σ_{wind} playing a minor role in the total flux uncertainty (Table S3 and Table 1).

The climatological monthly and annual σ_{total} is shown in Fig.3. The maximum σ_{total} values in different oceanic regions are shown in Table S3. In most of the months, it can be seen that the oceanic regions where σ_{total} is maximum, at the same oceanic regions σ_{DMS} is maximum while for some of the months σ_k is maximum. So, there is big contribution in σ_{total} by both σ_{DMS} and σ_k but for most of the regions σ_{DMS} shows primary contribution while σ_{wind} has minor contribution. In Fig.3, the regions where the σ_{total} is dominated by the variation in seawater DMS concentrations, i.e., $\sigma_{DMS} > \sigma_k$, are indicated by red dots. The regions

where the red dots are absent are the ones where the dominant contribution to σ_{total} is due to σ_k. Also, σ_{total} in oligotrophic oceans and most of the coastal areas are dominated by σ_{DMS}. Annually, the σ_{total} in the Southern Ocean is dominated by σ_{DMS}, but the coastal area of Antarctica is dominated by σ_k. Table 1 also shows the total DMS$_{sulfur}$ flux to the atmosphere according to each month and annually averaged. For most of the year, the total flux from regions where σ_{DMS} is greater than σ_k is larger. Indeed, the total annual flux of DMS$_{sulfur}$ to the atmosphere is estimated as 22.08 Tg, of which 17.16 Tg is contributed by areas where $\sigma_k < \sigma_{DMS}$. This indicates that on an annual scale, the uncertainty in DMS$_{sulfur}$ emissions is dominated by seawater DMS concentration. However, from Fig.3, the choice of the flux parametrization also contributes a considerable amount of uncertainty in the coastal areas of Antarctica, which can be seen in November, December, January, and February. Overall, the choice of seawater DMS estimation method has larger influence on sea-air DMS flux than the choice of flux parameterization, which is also corroborated by analysis presented by Bhatti et.al. (2023) and Tesdal et al. (2016).

3.4 Comparison with in situ observations

In situ DMS flux data were compared with the co-located DMS flux data estimated from different parameterizations using the H22 (Fig.4), G18 (Fig.S13), and W20 (Fig.S14). The raw in situ data points are localized and inconsistent in terms of temporal and spatial resolution while models provide the average. So, raw in situ flux data points are not comparable with the model flux values calculated with parametrizations. Hence, for the analysis, raw in situ DMS flux data is binned to 1º × 1º resolution grid box for each month and then flux data points within that box is averaged. Due to binning and averaging localized in situ information may be lost but for the comparison with DMS flux calculated with parametrization models this is the nearest traditional method for comparisons. After this, ordinary least square regression is applied. For reference, raw in situ DMS flux points are shown in the background (Fig.4, S13 and S14). All flux estimates using either of the DMS seawater climatologies, with any of the flux parameterizations, struggle to match the observations.

In most cases, the flux estimations in the lower range ($< 20\,\mu\mathrm{mol\,m^{-2}\,d^{-1}}$) are overestimated, while the values are underestimated in the higher range ($> 20\,\mu\mathrm{mol\,m^{-2}\,d^{-1}}$). Indeed, in all the cases, a positive intercept in the linear regressions shows that the emissions are overestimated at lower flux values. This would indicate a constant background flux in the estimated emissions, which would overestimate the total DMS$_{sulfur}$ flux to the atmosphere. In contrast, the fact that the flux estimates do not reproduce the higher DMS fluxes indicates that high emission scenarios, which would contribute strongly to new particle formation and growth, are underestimated by the emission estimations. It should be noted that we use monthly seawater DMS concentration fields as input. Hence, a difference between the observations and estimations is expected, but there is consistent overestimation of model flux for lower range ($0.1 - 20\,\mu\mathrm{mol\,m^{-2}\,d^{-1}}$) in situ flux points and underestimation for higher range ($20 - 50\,\mu\mathrm{mol\,m^{-2}\,d^{-1}}$) in situ flux points. The best match in the lower range is found when using the W20 seawater DMS estimations (Fig.S14), although the slope is consistently lower than 0.33, and the intercept is higher than 2.17 for all the flux parameterizations ($R^2 < 0.32$ for all the parameterizations). Both H22 and W20 perform better than G18, but none of the

correlation coefficients are found to be important, and all the flux parametrization methods fail to reproduce the in situ DMS flux values, particularly the high values of fluxes (Fig.4, S13 and S14).

4 Discussion

This study has been conducted to quantify the factors that contribute to the total uncertainty in DMS fluxes to the atmosphere. From our analysis, it was found that the total uncertainty in the DMS fluxes is dominated by the uncertainty in the seawater DMS concentrations, followed by the coefficient of gas transfer velocity used in flux parametrization equations. The uncertainty due to winds peed is negligible in comparison.

The sea water DMS concentrations estimated by G18, W20 and H22 have large differences between themselves (please check Joge: Part A). This is a major source of uncertainty and shows the need for more detailed long-term observations across different ocean basins. The present available observations are not consistent in terms of temporal and spatial resolution and some regions like the Southern Ocean are highly under sampled but very important due to high DMS emissions. Hence, models do not fully capture the seawater DMS variations, which translate into uncertainty in the emissions.

In addition to seawater DMS observations, which we hope will be undertaken in future, there are some regions where uncertainty in the total DMS flux is mostly due to the k values. From k vs u plots (Figs. S1-S7) of the seven flux parametrization methods, it is seen that there are large differences among these seven methods. In LM86, N00a, N00b, GM12 and W14 there is a spread in the values of k due to the Sc values used. This spread arises from the SST. Even though E93 uses this Sc, the spread is smaller compared to other parametrization, while there is negligible spread in Ho06. To calculate the DMS flux at present we do not use the C_a values as we assume that DMS is supersaturated in seawater. However, past studies have shown that in some special cases, such as when the atmospheric boundary layer is shallow on cold nights or in winter, it is important to consider the airside DMS concentration. In one of the model study, it was found that the difference in the emissions on considering C_a can be as high as 50% (Steiner and Denman, 2008; Steiner et al., 2006), which adds to the uncertainty. The k vs u plots are comparable between the seven parameterizations and the total uncertainty due to windspeed from different sources is negligible. Like in situ DMS observations, in situ flux observations are important in order to develop more accurate flux parametrizations. Observations collected from the different flux techniques like eddy covariance, gradient flux, etc. can add to the uncertainty in flux observation data and cross-comparison between the methods across a range of fluxes needs to be undertaken.

The gas transfer velocity equation of W14 uses the square of the average neutral stability winds at 10 m height or second moment i.e., average of the quadratic windspeed. In this study, we used monthly average windspeed i.e., the quadratic of average windspeed for W14. The first method of calculation will estimate higher k values than the second one due to the averaging of the winds. We checked the differences between the two and found that the maximum difference is not more than 4.3 cm h^{-1} for June, July and August months and it is less than 2 cm h^{-1} for rest of the year, which does not contribute pointedly to the large uncertainty.

The DMS flux derived from both empirical and prognostic models shows the poor agreement with fluxes from the point observations (Tesdal et al., 2016), which can also be seen with the flux parametrization methods used in this study when compared with the in situ DMS flux observations (Fig. 4). Tesdal et al.(2016) also concluded that there is large uncertainty in the temporal and spatial distribution of DMS concentrations and fluxes. The total sea-air DMS flux depends primarily on global mean surface ocean DMS concentrations, and the spatial distribution of DMS concentration and the magnitude of the gas exchange coefficient are of secondary importance. In our study, it is primarily seawater DMS concentrations that needs to estimated accurately as σ_{DMS} dominates over σ_k at most of the regions of global ocean but for some regions it is important to consider σ_k over σ_{DMS}, which agrees with the study of Tesdal et al.(2016).

5 Conclusions

The sea-air DMS flux was estimated using different seawater DMS climatologies (see Joge: Part A), wind, and SST as input to seven different flux parameterizations. All the flux estimations show a similar seasonal variation, with peaks in the summers of each hemisphere. However, there were large geographical and absolute flux differences among the different estimations, showing that the DMS_{sulfur} flux to the atmosphere is sensitive to the chosen seawater DMS fields and the chosen flux parameterization. The total uncertainty in flux estimation is dominated by the uncertainty in seawater DMS concentrations and the choice of flux parametrization, while the effect on the total uncertainty due to the different sources of wind speed is less important; however, this might not be true when comparing to in situ fluxes as the gustiness of wind might play an important role. In certain parts of the globe, such as the Peru upwelling region, the South Pacific Ocean, Indian Ocean, Arabian Sea, Bay of Bengal, Coastal areas, North Atlantic Ocean, Gulf of Alaska, and Southern Ocean, etc., the differences between the climatological estimated DMS of G18, W20, H22 is seen in the figures (Paper: Part A). Hence, the uncertainty in the total flux emission is dominated by the uncertainty due to the seawater DMS concentration in these areas where the differences are important (Fig.3). In other regions, uncertainty is dominated by the choice in the coefficient of the flux parametrization, such as the coastal area of Antarctica and the Arctic Ocean. A comparison of in situ and co-located estimated flux showed that all the parameterizations overestimate the DMS flux below 20 µmol m^{-2} d^{-1} but underestimate fluxes larger than 20 µmol m^{-2} d^{-1}. This suggests that emissions in current models overestimate the total sea-air DMS flux but underestimate the higher range (20 – 50 µmol m^{-2} d^{-1}) when it can impact new particle formation and growth.

Code availability

Codes for the analysis and figures are available on request.

Data availability

All the data used here are publicly available and links are provided in the manuscript.

Competing Interests

The authors declare that they have no conflict of interest.

Author Contributions

ASM conceptualized the study. SJ analyzed the data with help from SH. CM, MG, MY, TB and RS helped with the data, ideas and understanding of the study. SJ and ASM wrote the manuscript with the help of all the coauthors.

Acknowledgements

The Indian Institute of Tropical Meteorology is funded by the Ministry of Earth Sciences, Government of India. MG and RS acknowledge support from the European Research Council (ERC) under the European Union's Horizon 2020 research and innovation program (grant agreement #834162, SUMMIT Advanced Grant to RS), and the Spanish Government through grant GOOSE (PID2022_140872NB_I00) as well as the "Severo Ochoa Centre of Excellence" accreditation grant CEX2019-000928-S.

References

Abbatt, J. P. D., Leaitch, W. R., Aliabadi, A. A., Bertram, A. K., Blanchet, J., Boivin-rioux, A., Bozem, H., Burkart, J., Chang, R. Y. W., Charette, J., Chaubey, J. P., Fletcher, C. G., Galí, M., Ghahremaninezhad, R., Girard, E., and Gong, W.: Overview paper : New insights into aerosol and climate in the Arctic, Atmos. Chem. Phys., 19, 2527–2560, https://doi.org/10.5194/acp-19-2527-2019, 2019.

Andreae, M. O. and Barnard, W. R.: The marine chemistry of dimethylsulfide, Mar. Chem., 14, 267–279, https://doi.org/10.1016/0304-4203(84)90047-1, 1984.

Andreae, M. O. and Crutzen, P. J.: Atmospheric aerosols: Biogeochemical sources and role in atmospheric chemistry, Science (80-.)., 276, 1052–1058, 1997.

Andreae, M. O. and Raemdonck, H.: Dimethylsulfide in the surface ocean and the marine atmosphere: A Global View, Science (80-.)., 221, 744–747, 1983.

Bell, T. G., Landwehr, S., Miller, S. D., De Bruyn, W. J., Callaghan, A. H., Scanlon, B., Ward, B., Yang, M., and Saltzman, E. S.: Estimation of bubble-mediated air-sea gas exchange from concurrent DMS and CO2 transfer velocities at intermediate-high wind speeds, Atmos. Chem. Phys., 17, 9019–9033, https://doi.org/10.5194/acp-17-9019-2017, 2017.

Bhatti, Y. A., Revell, L. E., Schuddeboom, A. J., McDonald, A. J., Archibald, A. T., Williams, J., Venugopal, A. U., Hardacre, C., and Behrens, E.: The sensitivity of Southern Ocean atmospheric dimethyl sulfide (DMS) to modeled oceanic DMS concentrations and emissions, Atmos. Chem. Phys., 23, 15181–15196, https://doi.org/10.5194/acp-23-15181-2023, 2023.

Blomquist, B. W., Brumer, S. E., Fairall, C. W., Huebert, B. J., Zappa, C. J., Brooks, I. M., Yang, M., Bariteau, L.,

Prytherch, J., Hare, J. E., Czerski, H., Matei, A., and Pascal, R. W.: Wind Speed and Sea State Dependencies of Air-Sea Gas
395   Transfer: Results From the High Wind Speed Gas Exchange Study (HiWinGS), J. Geophys. Res. Ocean., 122, 8034–8062,
https://doi.org/10.1002/2017JC013181, 2017.

Carpenter, L. J., Archer, S. D., and Beale, R.: Ocean-atmosphere trace gas exchange, Chem. Soc. Rev., 41, 6473–506,
https://doi.org/10.1039/c2cs35121h, 2012.

Cember, R.: Bomb radiocarbon in the Red Sea: A medium-scale gas exchange experiment, J. Geophys. Res., 94, 2111,
400   https://doi.org/10.1029/JC094iC02p02111, 1989.

Charlson, R. J., Lovecook, J. E., Andreae, M. O., and Warren, S. G.: Ocean phytoplankton, atmospheric sulfur, cloud albdeo
and climate, Nature, 326, 655–661, https://doi.org/10.1029/2003GB002183, 1987.

Coale, K. H., Johnson, K. S., Fitzwater, S. E., Gordon, R. M., Tanner, S., Chavez, F. P., Ferioli, L., Sakamoto, C., Rogers,
P., Millero, F., Steinberg, P., Nightingale, P., Cooper, D., Cochlan, W. P., Landry, M. R., Constantinou, J., Rollwagen, G.,
405   Trasvina, A., and Kudela, R.: A massive phytoplankton bloom induced by an ecosystem-scale iron fertilization experiment
in the equatorial Pacific Ocean, Nature, 383, 495–501, https://doi.org/10.1038/383495a0, 1996.

D'Asaro, E. and McNeil, C.: Air-sea gas exchange at extreme wind speeds measured by autonomous oceanographic floats
(DOI:10.1016/j.jmarsys.2006.06.007), J. Mar. Syst., 74, 722–736, https://doi.org/10.1016/j.jmarsys.2008.02.006, 2008.

Dacey, J. W. H. and Wakeham, G.: HENRY'S LAW CONSTANTS FOR DIHETHYLSULFIDE IN FRESHWATER AND
410   SEAWATER, October, 11, 991–994, 1984.

Erickson, D. J.: A stability dependent theory for air-sea gas exchange, J. Geophys. Res. Ocean., 98, 8471–8488,
https://doi.org/10.1029/93JC00039, 1993.

Frew, N. M., Bock, E. J., Schimpf, U., Hara, T., Haußecker, H., Edson, J. B., McGillis, W. R., Nelson, R. K., McKenna, S.
P., Uz, B. M., and Jähne, B.: Air-sea gas transfer: Its depedence on wind stress, small-scale roughness, and surface films, J.
415   Geophys. Res. Ocean., 109, 1–23, https://doi.org/10.1029/2003JC002131, 2004.

Galí, M. and Simó, R.: A meta-analysis of oceanic DMS and DMSP cycling processes: Disentangling the summer paradox,
Global Biogeochem. Cycles, 29, 496–515, https://doi.org/10.1002/2014GB004940, 2015.

Galí, M., Levasseur, M., Devred, E., Simó, R., and Babin, M.: Sea-surface dimethylsulfide (DMS) concentration from
satellite data at global and regional scales, Biogeosciences, 15, 3497–3519, https://doi.org/10.5194/bg-15-3497-2018, 2018.

420   Goddijn-Murphy, L., Woolf, D. K., and Marandino, C. A.: Space-based retrievals of air-sea gas transfer velocities using
altimeters: Calibration for dimethyl sulfide, J. Geophys. Res. Ocean., 117, n/a-n/a, https://doi.org/10.1029/2011JC007535,
2012.

Ho, D. T., Law, C. S., Smith, M. J., Schlosser, P., Harvey, M., and Hill, P.: Measurements of air-sea gas exchange at high
wind speeds in the Southern Ocean: Implications for global parameterizations, Geophys. Res. Lett., 33, L16611,
425   https://doi.org/10.1029/2006GL026817, 2006.

Hulswar, S., Simó, R., Galí, M., Bell, T. G., Lana, A., Inamdar, S., Halloran, P. R., Manville, G., and Mahajan, A. S.: Third
revision of the global surface seawater dimethyl sulfide climatology (DMS-Rev3), Earth Syst. Sci. Data, 14, 2963–2987,

https://doi.org/10.5194/essd-14-2963-2022, 2022.

Ishii, M., Shouji, A., Sugimoto, S., and Matsumoto, T.: Objective analyses of sea-surface temperature and marine meteorological variables for the 20th century using ICOADS and the Kobe Collection, Int. J. Climatol., 25, 865–879, https://doi.org/10.1002/joc.1169, 2005.

Jahne, B., Münnich, K. O., and Siegenthaler, U.: Measurements of gas exchange and momentum transfer in a circular wind-water tunnel, Tellus, 31, 321–329, https://doi.org/10.3402/tellusa.v31i4.10440, 1979.

Jähne, B., Huber, W., Dutzi, A., Wais, T., and Ilmberger, J.: Wind/Wave-Tunnel Experiment on the Schmidt Number — and Wave Field Dependence of Air/Water Gas Exchange, in: Gas Transfer at Water Surfaces, Springer Netherlands, Dordrecht, 303–309, https://doi.org/10.1007/978-94-017-1660-4_28, 1984.

Jardine, K., Yañez-Serrano, A. M., Williams, J., Kunert, N., Jardine, A., Taylor, T., Abrell, L., Artaxo, P., Guenther, A., Hewitt, C. N., House, E., Florentino, A. P., Manzi, A., Higuchi, N., Kesselmeier, J., Behrendt, T., Veres, P. R., Derstroff, B., Fuentes, J. D., Martin, S. T., and Andreae, M. O.: Dimethyl sulfide in the Amazon rain forest, Global Biogeochem. Cycles, 29, 1–14, https://doi.org/10.1002/2014GB004969, 2015.

Jin, Q., Grandey, B. S., Rothenberg, D., Avramov, A., and Wang, C.: Impacts on cloud radiative effects induced by coexisting aerosols converted from international shipping and maritime DMS emissions, Atmos. Chem. Phys., 18, 16793–16808, https://doi.org/10.5194/acp-18-16793-2018, 2018.

Kalnay, E., Kanamitsu, M., Kistler, R., Collins, W., Deaven, D., and Gandin, L.: The NCEP / NCAR 40-Year Reanalysis Project, Bull. Am. Meteorol. Soc., 437–472, https://doi.org/10.1175/1520-0477(1996)077<0437:TNYRP>2.0.CO;2, 1996.

Kettle, A. J. and Andreae, M. O.: Flux of dimethylsulfide from the oceans: a comparison of updated data sets and flux models, J Geophys Res, 105, 2000.

Lana, A., Bell, T. G., Simó, R., Vallina, S. M., Ballabrera-Poy, J., Kettle, a. J., Dachs, J., Bopp, L., Saltzman, E. S., Stefels, J., Johnson, J. E., and Liss, P. S.: An updated climatology of surface dimethlysulfide concentrations and emission fluxes in the global ocean, Global Biogeochem. Cycles, 25, https://doi.org/10.1029/2010GB003850, 2011.

Liss, P. S. and Merlivat, L.: The Role of Air-Sea Exchange in Geochemical Cycling, JI3-127. © 1986 by D. Reidel Publishing Company., 1983, 113–127, 1983.

Liss, P. S. and Merlivat, L.: Air-Sea Gas Exchange Rates: Introduction and Synthesis, in: The Role of Air-Sea Exchange in Geochemical Cycling, vol. 1983, Springer Netherlands, Dordrecht, 113–127, https://doi.org/10.1007/978-94-009-4738-2_5, 1986.

Mahajan, A. S., Fadnavis, S., Thomas, M. A., Pozzoli, L., Gupta, S., Royer, S., Saiz-Lopez, A., and Simó, R.: Quantifying the impacts of an updated global dimethyl sulfide climatology on cloud microphysics and aerosol radiative forcing, J. Geophys. Res. Atmos., 120, 1–13, https://doi.org/10.1002/2014JD022687, 2015.

Marandino, C. A., Bruyn, W. J. De, Miller, S. D., and Saltzman, E. S.: Open ocean DMS air/sea fluxes over the eastern South Pacific Ocean, Atmos. Chem. Phys., 9, 345–356, 2009.

McNabb, B. J. and Tortell, P. D.: Improved prediction of dimethyl sulfide (DMS) distributions in the northeast subarctic

Pacific using machine-learning algorithms, Biogeosciences, 19, 1705–1721, https://doi.org/10.5194/bg-19-1705-2022, 2022.

Monahan, E. C. and Spillane, M. C.: The Role of Oceanic Whitecaps in Air-Sea Gas Exchange, in: Gas Transfer at Water Surfaces, Springer Netherlands, Dordrecht, 495–503, https://doi.org/10.1007/978-94-017-1660-4_45, 1984.

465   Nightingale, D., Malin, G., Law, C. S., Watson, J., Liss, S., and Liddicoat, I.: In situ evaluation of air-sea gas exchange parameterizations using novel conservative and volatile tracers., Global Biogeochem. Cycles, 14, 373–387, https://doi.org/10.1029/1999GB900091, 2000.

Omori, Y., Tanimoto, H., Inomata, S., Ikeda, K., Iwata, T., Kameyama, S., Uematsu, M., Gamo, T., Ogawa, H., and Furuya, K.: Sea-to-air flux of dimethyl sulfide in the South and North Pacific Ocean as measured by proton transfer reaction-mass

470   spectrometry coupled with the gradient flux technique, J. Geophys. Res., 122, 7216–7231, https://doi.org/10.1002/2017JD026527, 2017.

Pazmiño, A. F., Godin-Beekmann, S., Ginzburg, M., Bekki, S., Hauchecorne, A., Piacentini, R. D., and Quel, E. J.: Impact of Antarctic polar vortex occurrences on total ozone and UVB radiation at southern Argentinean and Antarctic stations during 1997-2003 period, J. Geophys. Res. D Atmos., 110, 1–13, https://doi.org/10.1029/2004JD005304, 2005.

475   Quinn, P. K. and Bates, T. S.: The case against climate regulation via oceanic phytoplankton sulphur emissions., Nature, 480, 51–6, https://doi.org/10.1038/nature10580, 2011.

Quinn, P. K., Coffman, D. J., Johnson, J. E., Upchurch, L. M., and Bates, T. S.: Small fraction of marine cloud condensation nuclei made up of sea spray aerosol, Nat. Geosci., 10, 674–679, https://doi.org/10.1038/ngeo3003, 2017.

Saltzman, E. S., King, D. B., Holmen, K., and Leck, C.: Experimental determination of the diffusion coefficient of

480   dimethylsulfide in water, J. Geophys. Res., 98, 16481, https://doi.org/10.1029/93JC01858, 1993.

Simó, R.: Production of atmospheric sulfur by oceanic plankton : biogeochemical , ecological and evolutionary links, Trends Ecol. Evol., 16, 287–294, 2001.

Simó, R. and Dachs, J.: Global ocean emission of dimethylsulfide predicted from biogeophysical data, Global Biogeochem. Cycles, 16, https://doi.org/10.1029/2001GB001829, 2002.

485   Steiner, N. and Denman, K.: Parameter sensitivities in a 1-D model for DMS and sulphur cycling in the upper ocean, Deep. Res. Part I Oceanogr. Res. Pap., 55, 847–865, https://doi.org/10.1016/j.dsr.2008.02.010, 2008.

Steiner, N., Denman, K., McFarlane, N., and Solheim, L.: Simulating the coupling between atmosphere-ocean processes and the planktonic ecosystem during SERIES, Deep. Res. Part II Top. Stud. Oceanogr., 53, 2434–2454, https://doi.org/10.1016/j.dsr2.2006.05.030, 2006.

490   Tesdal, J. E., Christian, J. R., Monahan, A. H., and Von Salzen, K.: Evaluation of diverse approaches for estimating sea-surface DMS concentration and air-sea exchange at global scale, Environ. Chem., 13, 390–412, https://doi.org/10.1071/EN14255, 2016.

Del Valle, D. A., Kieber, D. J., Toole, D. A., Brinkley, J., and Kienea, R. P.: Biological consumption of dimethylsulfide (DMS) and its importance in DMS dynamics in the Ross Sea, Antarctica, Limnol. Oceanogr., 54, 785–798,

495   https://doi.org/10.4319/lo.2009.54.3.0785, 2009.

Vettikkat, L., Sinha, V., Datta, S., Kumar, A., Hakkim, H., Yadav, P., and Sinha, B.: Significant emissions of dimethyl sulfide and monoterpenes by big-leaf mahogany trees: Discovery of a missing dimethyl sulfide source to the atmospheric environment, Atmos. Chem. Phys., 20, 375–389, https://doi.org/10.5194/acp-20-375-2020, 2020.

Waewsak, J., Chancham, C., Landry, M., and Gagnon, Y.: An Analysis of Wind Speed Distribution at Thasala, Nakhon Si Thammarat, Thailand, J. Sustain. Energy Environ., 2, 51–55, 2011.

Wang, W.-L., Song, G., Primeau, F., Saltzman, E. S., Bell, T. G., and Moore, J. K.: Global ocean dimethyl sulfide climatology estimated from observations and an artificial neural network, Biogeosciences, 17, 5335–5354, https://doi.org/10.5194/bg-17-5335-2020, 2020.

Wanninkhof, R.: Relationship between wind speed and gas exchange over the ocean, J. Geophys. Res., 97, 7373–7382, https://doi.org/10.1029/92JC00188, 1992.

Wanninkhof, R.: Relationship between wind speed and gas exchange over the ocean revisited, Limnol. Oceanogr. Methods, 12, 351–362, https://doi.org/10.4319/lom.2014.12.351, 2014.

Wanninkhof, R., Asher, W., Weppernig, R., Chen, H., Schlosser, P., Langdon, C., and Sambrotto, R.: Gas transfer experiment on Georges Bank using two volatile deliberate tracers, J. Geophys. Res., 98, 20237, https://doi.org/10.1029/93JC01844, 1993.

Wanninkhof, R., Hitchcock, G., Wiseman, W. J., Vargo, G., Ortner, P. B., Asher, W., Ho, D. T., Schlosser, P., Dickson, M.-L., Masserini, R., Fanning, K., and Zhang, J.-Z.: Gas exchange, dispersion, and biological productivity on the West Florida Shelf: Results from a Lagrangian Tracer Study, Geophys. Res. Lett., 24, 1767–1770, https://doi.org/10.1029/97GL01757, 1997.

Watson, A. J., Upstill-Goddard, R. C., and Liss, P. S.: Air–sea gas exchange in rough and stormy seas measured by a dual-tracer technique, Nature, 349, 145–147, https://doi.org/10.1038/349145a0, 1991.

Woodhouse, M. T., Carslaw, K. S., Mann, G. W., Vallina, S. M., Vogt, M., Halloran, P. R., and Boucher, O.: Low sensitivity of cloud condensation nuclei to changes in the sea-air flux of dimethyl-sulphide, Atmos. Chem. Phys., 10, 7545–7559, 2010.

Xu, F., Jin, N., Ma, Z., Zhang, H. H., and Yang, G. P.: Distribution, Occurrence, and Fate of Biogenic Dimethylated Sulfur Compounds in the Yellow Sea and Bohai Sea During Spring, J. Geophys. Res. Ocean., 124, 5787–5800, https://doi.org/10.1029/2019JC015085, 2019.

Yan, S. B., Li, X. J., Xu, F., Zhang, H. H., Wang, J., Zhang, Y., Yang, G. P., Zhuang, G. C., and Chen, Z.: High-resolution distribution and emission of dimethyl sulfide and its relationship with pCO2 in the Northwest Pacific Ocean, Front. Mar. Sci., 10, 1–12, https://doi.org/10.3389/fmars.2023.1074474, 2023.

Yang, G., Song, Y., Zhang, H., Li, C., and Wu, G.: Seasonal variation and biogeochemical cycling of dimethylsulfide (DMS) and dimethylsulfoniopropionate (DMSP) in the Yellow Sea and Bohai Sea, J. Geophys. Res. Ocean., 119, 8897–8915, https://doi.org/10.1002/2014JC010373, 2014.

Yang, G. P., Zhang, S. H., Zhang, H. H., Yang, J., and Liu, C. Y.: Distribution of biogenic sulfur in the Bohai Sea and northern Yellow Sea and its contribution to atmospheric sulfate aerosol in the late fall, Mar. Chem., 169, 23–32,

530   https://doi.org/10.1016/j.marchem.2014.12.008, 2015.

Yang, Y., Wang, H., Smith, S. J., Easter, R., Ma, P., Qian, Y., Yu, H., Li, C., and Rasch, P. J.: Global source attribution of sulfate concentration and direct and indirect radiative forcing, Atmos. Chem. Phys., 17, 8903–8922, https://doi.org/10.5194/acp-17-8903-2017, 2017.

Yi, Z., Wang, X., Sheng, G., and Fu, J.: Exchange of carbonyl sulfide (OCS) and dimethyl sulfide (DMS) between rice

535   paddy fields and the atmosphere in subtropical China, Agric. Ecosyst. Environ., 123, 116–124, https://doi.org/10.1016/j.agee.2007.05.011, 2008.

Yoch, D. C.: Dimethylsulfoniopropionate: Its sources, role in the marine food web, and biological degradation to dimethylsulfide, Appl. Environ. Microbiol., 68, 5804–5815, https://doi.org/10.1128/AEM.68.12.5804-5815.2002, 2002.

Zavarsky, A., Goddijn-Murphy, L., Steinhoff, T., and Marandino, C. A.: Bubble-Mediated Gas Transfer and Gas Transfer

540   Suppression of DMS and CO2, J. Geophys. Res. Atmos., 123, 6624–6647, https://doi.org/10.1029/2017JD028071, 2018.

Zhai, X., Song, Y. C., Li, J. L., Yang, J., Zhang, H. H., and Yang, G. P.: Distribution Characteristics of Dimethylated Sulfur Compounds and Turnover of Dimethylsulfide in the Northern South China Sea During Summer, J. Geophys. Res. Biogeosciences, 125, 1–14, https://doi.org/10.1029/2019JG005363, 2020.

Zhang, M., Marandino, C. A., Yan, J., Wu, Y., Park, K., Sun, H., Gao, Z., and Xu, S.: Unravelling Surface Seawater DMS

545   Concentration and Sea-To-Air Flux Changes After Sea Ice Retreat in the Western Arctic Ocean, Global Biogeochem. Cycles, 35, 1–15, https://doi.org/10.1029/2020GB006796, 2021.

Zhao, D., Toba, Y., Suzuki, Y., and Komori, S.: Effect of wind waves on air's ea gas exchange: proposal of an overall CO 2 transfer velocity formula as a function of breaking-wave parameter , Tellus B Chem. Phys. Meteorol., 55, 478–487, https://doi.org/10.3402/tellusb.v55i2.16747, 2003.

550   Zhao, J., Zhang, Y., Bie, S., Yang, G., Bilsback, K. R., Pierce, J. R., and Chen, Y.: Improving Estimates of Dynamic Global Marine DMS and Implications for Aerosol Radiative Effect, J. Geophys. Res. Atmos., 129, 1–18, https://doi.org/10.1029/2023JD039314, 2024.

555

Tables :

Table 1. Area Weighted Global mean flux standard deviation for each month and annually due to σ_{DMS}, σ_k and σ_{wind}. Also, DMS$_{Sulfur}$ emissions for each month and annually from the areas with $\sigma_{DMS} > \sigma_k$ and the area $\sigma_{DMS} < \sigma_k$ and the total emission across the globe is computed using the N00b flux parameterization and H22 DMS climatology.

Month	Area Weighted Global Mean Flux std. due to σ_{DMS} (μmol m^{-2} d^{-1})	Area Weighted Global Mean Flux std. due to σ_k (μmol m^{-2} d^{-1})	Area Weighted Global Mean Flux std. due to σ_{wind} (μmol m^{-2} d^{-1})	DMS$_{Sulfur}$ emissions where $\sigma_{DMS} > \sigma_k$ (Tg)	DMS$_{Sulfur}$ emissions where $\sigma_{DMS} < \sigma_k$ (Tg)	Total DMS$_{Sulfur}$ emissions (Tg)
January	1.85	1.69	0.16	1.47	0.85	2.33
February	1.42	1.29	0.13	1.07	0.68	1.74
March	1.52	1.28	0.13	1.54	0.50	2.04
April	1.07	0.99	0.10	0.98	0.52	1.50
May	1.31	1.09	0.11	1.11	0.51	1.62
June	1.51	1.09	0.11	1.24	0.49	1.73
July	1.39	1.09	0.12	1.29	0.52	1.81
August	1.41	1.08	0.12	1.42	0.47	1.89
September	1.04	0.83	0.09	1.09	0.41	1.50
October	1.08	0.94	0.10	0.97	0.63	1.60
November	1.79	1.47	0.14	1.36	0.60	1.96
December	1.82	1.70	0.16	1.40	0.90	2.30
Annual	**1.44**	**1.21**	**0.12**	**17.16**	**4.93**	**22.08**
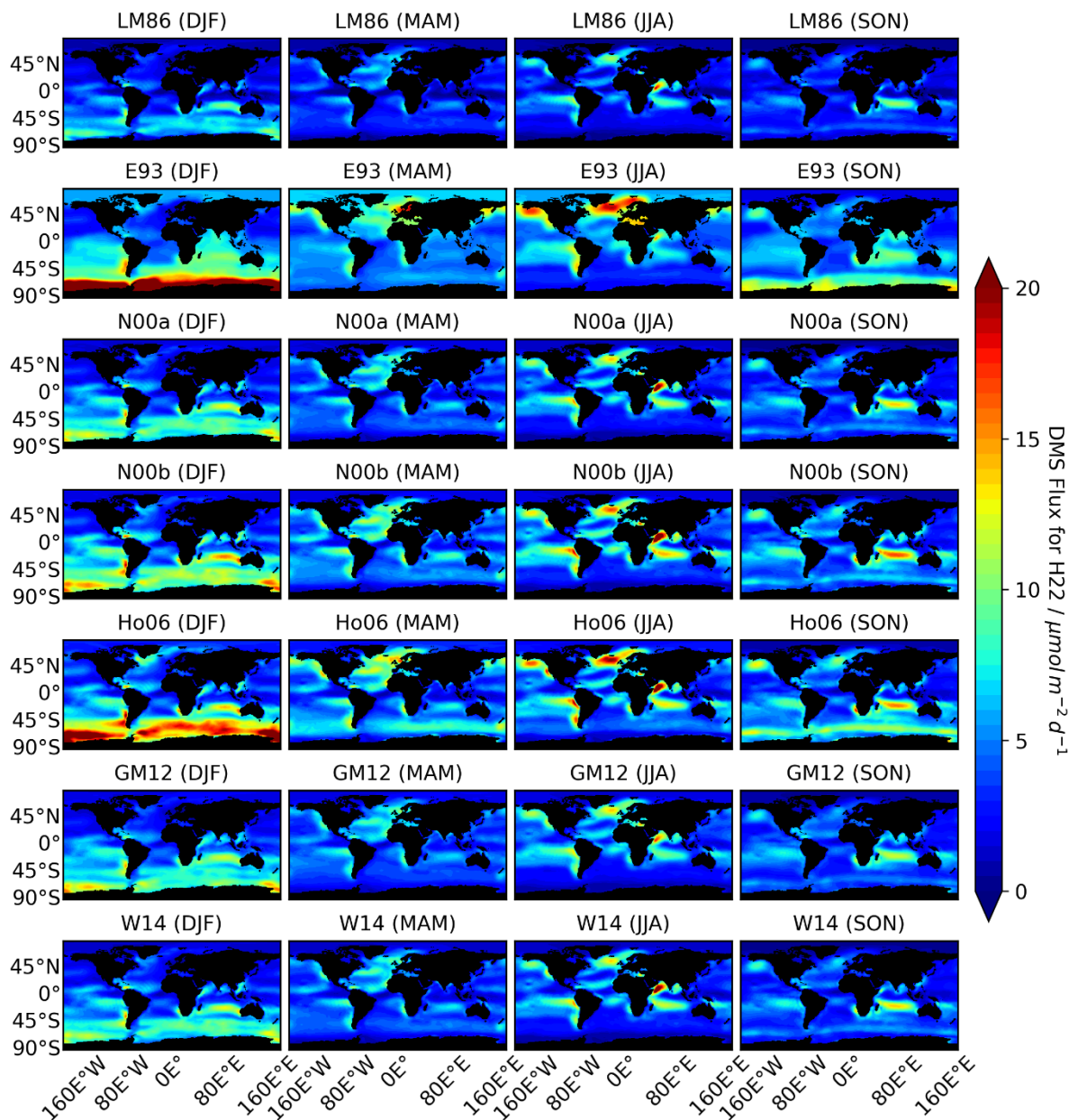
Figures :

Figure 1: DMS fluxes estimated using the seven parameterizations for different seasons using the H22 climatology. The geographical pattern is similar in all the estimates, although the absolute values differ according to the parameterization chosen. In June-July-August (JJA),a maximum flux of 33.75 µmol m^{-2} d^{-1} is calculated in Indian ocean near Somalia with N00b. In December-January-February (DJF),a maximum flux of 45.82 µmol m^{-2} d^{-1} is calculated in Weddell Sea region with E93.
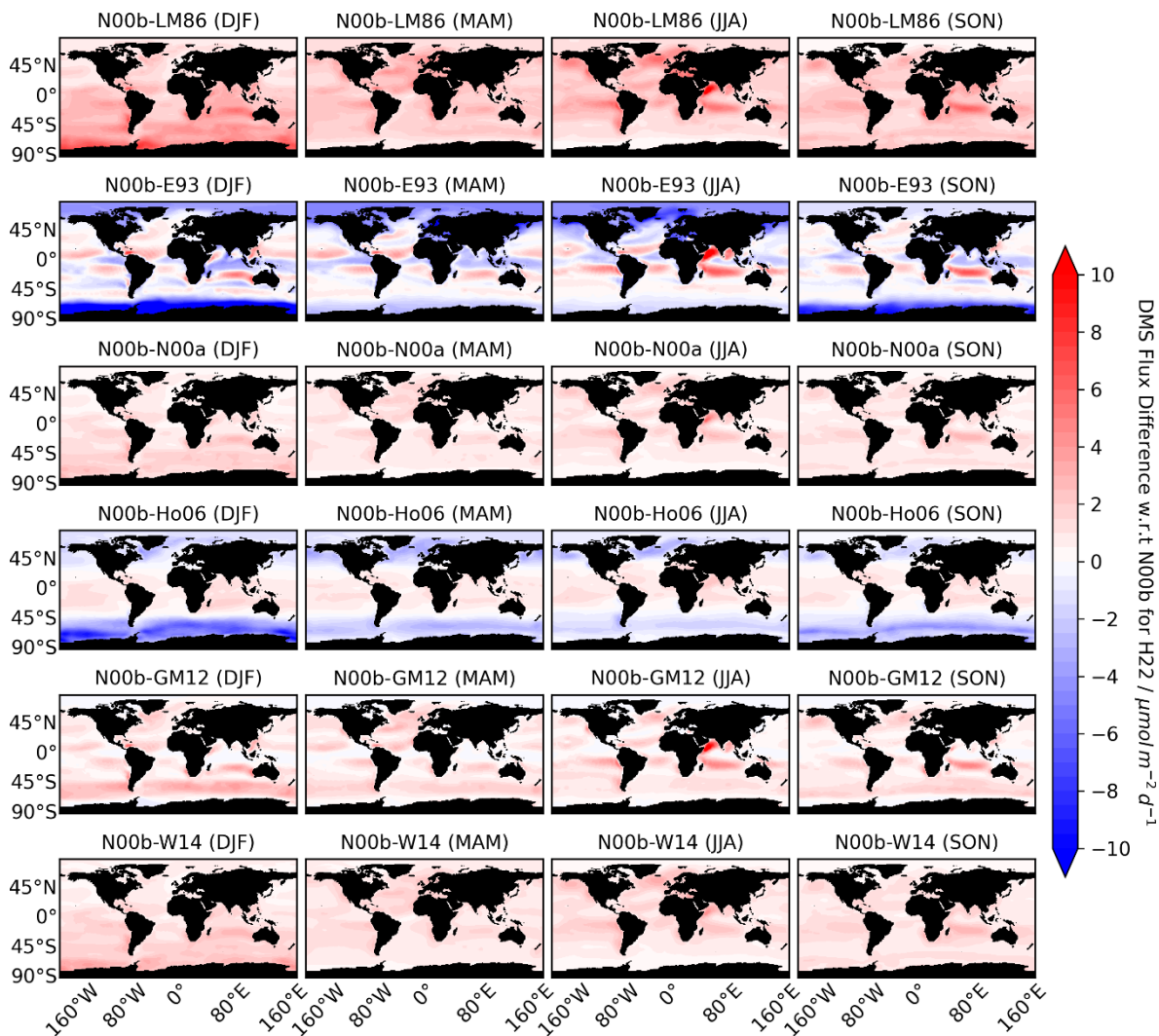
Figure 2: Differences between the DMS fluxes estimated using H22 with the N00b parameterization and the other seven parameterizations. For all the seasons (December-January-February (DJF),March-April-May (MAM), June-July-August (JJA), September-October-November (SON)), N00b-LM86 shows a positive difference, while the other parameterizations (E93, Ho06) show negative differences in the Southern Ocean and Arctic region, although some positive differences are also present in E93 and Ho06 in mid latitude regions. GM12, W14 and N00a show small positive differences with N00b while N00b-LM86 shows notable large positive difference. The summary of the differences in different oceanic regions is listed in Table S2.

580
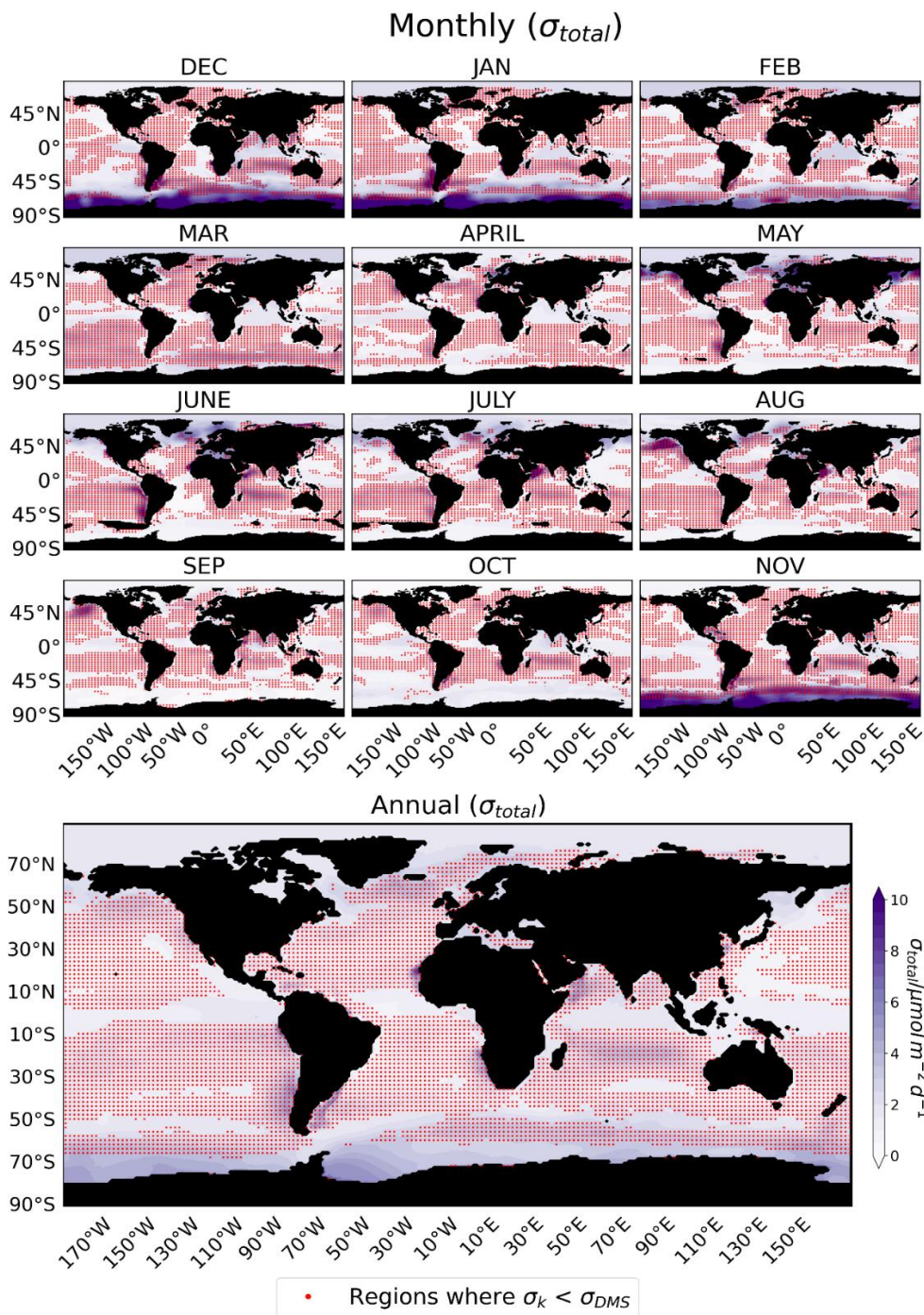
585   **Figure 3:** An estimate of the total variation (σ_{total}) in the flux emission, which is shown as a background map and is obtained from the standard deviations in the seawater DMS concentrations (σ_{DMS}), standard deviations in the coefficients of parametrizations (σ_k) and variation due to wind speed (σ_{wind}). σ_{wind} has a small contribution compared to σ_{DMS} and σ_k (Table 1). The regions where seawater DMS concentrations drive the uncertainty are indicated by red dots ($\sigma_{DMS} > \sigma_k$), while in the other areas (no red dots), it is driven by the variation due to the choice of the flux parameterization ($\sigma_{DMS} < \sigma_k$). The maximum values of σ_{total} is listed in Table S3.
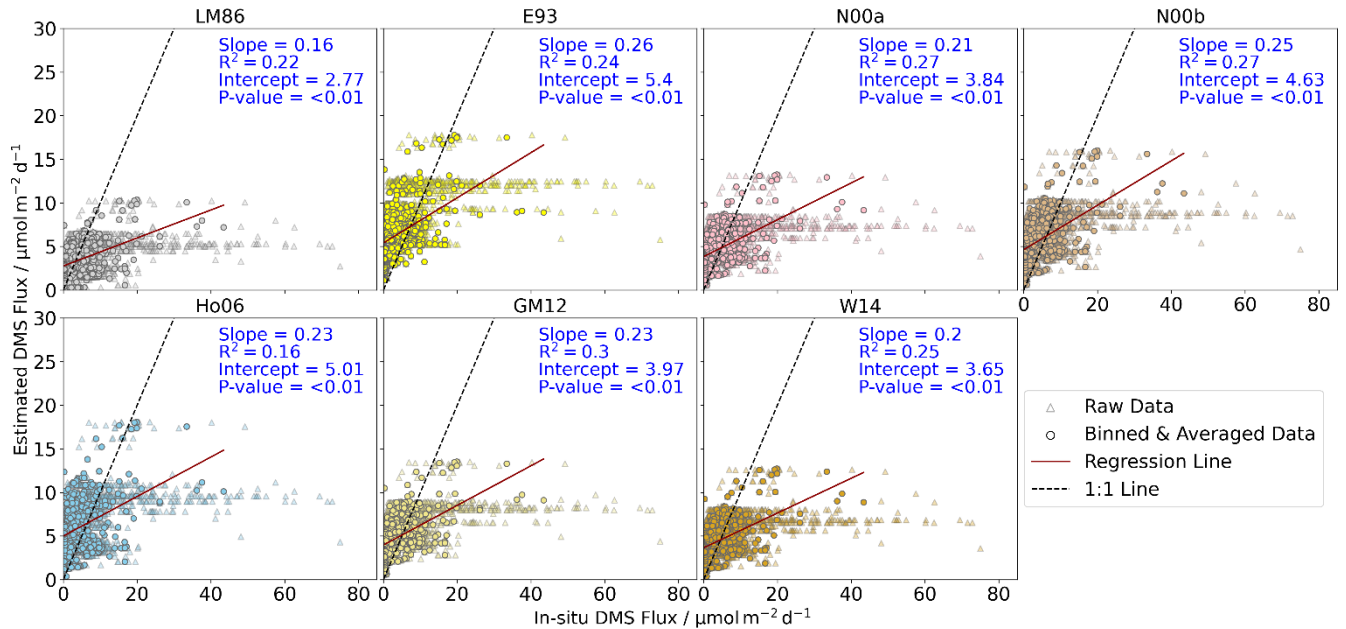
590

Figure 4: Comparison of in situ and estimated DMS fluxes (using H22) with the different parameterizations. Here, the regression analysis is done with binned and averaged in situ data at 1°×1° resolution, as the flux climatologies are also at the same resolution. The analysis shows that flux calculations result in higher fluxes than observations at low levels (< 20 µmol m^{-2} d^{-1}) and lower fluxes than observations at higher levels (> 20 µmol m^{-2} d^{-1}),which indicates that flux parametrization methods fail to represent the range accurately. The black dash line is the

595   1:1 representation between in situ and the estimated DMS flux points, and the dark red line is the regression line. A list of the in situ observations used for the comparison is given in Table S1.